Theoretical study of the mechanism of H_2O^+ dissociative recombination

Sifiso M. Nkambule and Åsa Larson
Department of Physics, Stockholm University, SE-106 91 Stockholm, Sweden

Samantha Fonseca dos Santos and Ann E. Orel*
Department of Chemical Engineering and Materials Science, University of California, Davis, Davis, California 95616, USA

(Received 8 May 2015; published 30 July 2015)

By combining electronic structure and scattering calculations, quasidiabatic potential energy surfaces of both bound Rydberg and electronic resonant states of the water molecule are calculated at the multireference configuration-interaction level. The scattering matrix calculated at low collision energy is used to obtain explicitly all couplings elements responsible for the electronic capture to bound Rydberg states. These are used to estimate the cross section arising from the indirect mechanism of dissociative recombination. Additionally, the role of the direct capture and dissociation through the resonant states is explored using wave-packet propagation along one-dimensional slices of the multidimensional potential energy surfaces.

DOI: 10.1103/PhysRevA.92.012708 PACS number(s): 34.80.Ht, 34.80.Lx

I. INTRODUCTION

There have been a number of experimental studies of the dissociative recombination (DR) of the water ion. However, there are significantly fewer theoretical studies of this reaction. There are several unanswered questions about the mechanism and the dynamics of the DR process in this system. Here we take a first step toward a theoretical study of the reaction, attempting to obtain a better understanding of the process.

The first measurement of the total cross section was carried out in 1983 by Mul *et al.* [1]. The absolute cross sections of DR have been measured for both the H_2O^+ [1–3] and HDO^+ ions [2]. At low energies (<2 eV), the cross section decreases significantly faster than the E^{-1} behavior expected for the direct mechanism of DR [2]. Around 0.3–0.4 eV the cross section drops by a factor of 3, indicating the opening of a new autoionization channel. At higher collision energies, around 5 and 15 eV, there are pronounced peaks in the DR cross section that might reveal capture into higher-lying resonant states. The ratio of the HDO^+/H_2O^+ cross sections is about 0.6 and they display very similar energy dependences [2].

At zero collision energy, there are several dissociation channels open and the energetics of the DR process are shown below:

$$H_2O^+ + e^- \longrightarrow \begin{cases} O(^3P) + H_2 + 7.6\ \text{eV} \\ OH + H(^2S) + 7.5\ \text{eV} \\ O(^3P) + H(^2S) + H(^2S) + 3.04\ \text{eV} \\ O(^1D) + H(^2S) + H(^2S) + 1.07\ \text{eV}. \end{cases} \quad (1)$$

Here the energies are given for OH and H_2 in their electronic and vibrational ground states and with negligible rotational energy.

There are numerous measurements of the branching ratios. For DR of the water ion in the ground vibrational state, the three-body breakup dominates with measured ratios ranging from 0.57 ± 0.07 [2] to 0.73 ± 0.06 [3]. The propensity for three-body fragmentation is found in most experimental studies of DR on small molecular ions such as H_3^+ [4], NH_2^+ [5], and CH_2^+ [6]. No theoretical understanding of this observation is presently available. Interestingly, branching ratio measurements on the HDO^+ ion show that the OD+H channel is twice as probable as dissociation into OH+D [2].

Note that there are two three-body channels energetically open at zero collision energy, $O(^3P)$+H+H and $O(^1D)$+H+H. Using an imaging technique, the $O(^3P)/O(^1D)$ ratios have been measured at the CRYRING ion storage ring and found to be 3.5 ± 0.5 [7,8]. The recoil kinetic energy of the hydrogen atoms have been detected and different H-O-H angular distributions are observed depending on the excited state of the oxygen atom [7]. For breakup into the ground-state fragments, it is found that the angle either significantly increases or decreases during the dissociation dynamics [8].

In order to study the DR reaction theoretically, the potential energy surfaces of bound and resonant electronic states of H_2O must be computed. In this work, electron scattering calculations using the complex Kohn variational method [9] are combined with structure calculations using the multireference configuration-interaction method (see Sec. II A). From the electron scattering calculations, the autoionization widths of resonant states are computed. The resonant states are quasidiabatized as described below. As a first step toward understanding the mechanism of H_2O^+ DR, simplified models are applied to describe the direct and indirect processes. The direct capture and dissociation along the resonant states are modeled using one-dimensional wave-packet propagations, where either one or both bonds break while the H-O-H angle is frozen (see Sec. III A). No couplings between the electronic states are included and therefore we are not able to model the complicated dissociation dynamics and isotope dependence observed in the experiments. As outlined in Sec. III B, we perform electron-ion scattering calculations just above the ionization threshold and obtain all couplings elements directly from the scattering matrix calculated with the variational complex Kohn method. These are then used to compute the cross section for indirect DR.

Unless otherwise stated, atomic units are used throughout.

*aeorel@ucdavis.edu

II. COMPUTATIONAL DETAILS

A. Electronic-structure calculations

The $\tilde{X}\,^1A_1$ ground state of H_2O has the dominant configuration $(1a_1)^2(2a_1)^2(1b_2)^2(3a_1)^2(1b_1)^2$ in C_{2v} symmetry. The electron in the highest occupied molecular orbital is bound with 12.6 eV, which if removed leads to the formation of H_2O^+ in its $^2B_1$ ground state. There are two other low-lying ionic states corresponding to the removal of an electron in the $(3a_1)$ orbital leading to the $^2A_1$ and the $^2B_2$ formed by the removal of the $(1b_2)$ electron. The resonances seen in electron scattering from H_2O^+ are Rydberg states converging to these excited ionic states. They are crossed at large internuclear separations by states converging to even higher ionic excited states.

In this work, two sets of electronic structure calculations have been performed. The first of them was carried out to obtain Rydberg and resonant states involved in the direct DR process, therefore we were particularly interested in achieving a good description of the curve crossing between resonances and the ionic-core potential. The focus for the second set was on the indirect DR process and the calculations were optimized to describe as well as possible the ionic ground state and its Rydberg series at molecular geometries close to the equilibrium.

For the direct DR model, the potential energy surfaces of the ion as well as excited states of the neutral molecule are calculated using the multireference configuration-interaction (MRCI) method. This will provide us with the potential energy of the electronically bound states that are situated below the ground state of the ion. We also use the structure calculations to interpolate the potentials of the resonant states between the geometries where electron scattering calculations are performed. Note that although at equilibrium the molecule has C_{2v} symmetry, if the molecule is stretched asymmetrically the symmetry becomes C_s and a larger configuration-interaction (CI) calculation is needed. Calculations were carried out in both C_{2v} and C_s symmetries.

In order to describe both the Rydberg series converging to the various excited ionic states, which are the electronic resonances, and the bound Rydberg states, we first carried out a self-consistent-field (SCF) calculation on the neutral with a basis set consisting of $(4s,1p)$ primitive functions contracted to $[3s,1p]$ for the hydrogen and $(9s,7p,1d)$ contracted to $[4s,4p,1d]$ for the oxygen atom. In the next step, these SCF orbitals were used in a MRCI calculation on the three lowest states of the ion, where the lowest orbital [$(1a_1)$ in C_{2v} or $(1a')$ in C_s], mainly composed of the the $1s$ atomic orbital on oxygen, was frozen and the next four orbitals formed the active space. A full CI was done in the active space and single and double excitations from this set of configurations were allowed into the remaining orbitals. Natural orbitals were obtained from averaging the orbitals, over the lowest three ionic states. The natural orbitals were then further expanded by adding diffuse $(1s,1p)$ orbitals on oxygen and $(2s,2p)$ on hydrogen.

Then a MRCI calculation was carried out to determine the potential energy surfaces of the ground state of the ion as well as excited states of the neutral molecule. In these calculations, the lowest $(1a')$ core orbital was kept doubly occupied and the reference configurations were constructed by excitations of eight electrons (seven for the ion) among the seven orbitals: $(2a')$, $(3a')$, $(4a')$, $(5a')$, $(6a')$, $(1a'')$, and $(2a'')$. Single excitations out of the reference configurations were included.

A slightly different calculation was performed for the indirect DR description. The first difference is regarding the choice of the basis set. In the indirect DR model we used the cc-pVTZ basis set [10] centered on each atom and included all s, p, and d orbitals. The second change is with respect to the computation of the natural orbitals. Since in the indirect DR model only the knowledge of the Rydberg series converging to the ground state of the ion is relevant, the natural orbitals are obtained simply from a MRCI calculation on the ground ionic state. The reference configurations were generated by keeping the $(1a')$ core orbital doubly occupied and by allowing all possible excitations among the following eight orbitals. The last difference in the bound-state calculations is the choice of expansion basis. The Rydberg energies were obtained by further expanding the natural orbitals by adding at the center of charge the diffuse universal Rydberg Gaussian basis set $(8s,7p,6d)$ [11] to the initial Gaussian basis. Then the potential energy surfaces of the ion and the neutral system were generated using a MRCI calculation with an active space of eight orbitals (again keeping the core orbital frozen) and by allowing for single external excitations. By using this approach, we were able to obtain Rydberg states up to $n = 5$ and therefore guarantee the convergence of the quantum defects with respect to the principal quantum number.

B. Scattering calculations

The energy positions and autoionization widths of the electronic resonant states were determined using the complex Kohn variational method [9]. The trial wave function for the neutral [$(N + 1)$-electron] system is written as

$$\Psi_{\Gamma_0} = \sum_{\Gamma} A[\Phi_\Gamma F_{\Gamma\Gamma_0}] + \sum_{\mu} d_\mu^{\Gamma_0}\Theta_\mu. \qquad (2)$$

The first sum is defined as the P-space portion of the wave function and runs over the energetically open target states. Here the symbol index Γ labels all quantum numbers representing a physical scattering state, i.e., internal state of the target and angular momentum quantum numbers of the scattered electron; $\Phi_\Gamma(\mathbf{r}_1,\ldots,\mathbf{r}_N)$ represents the target wave function for the ion; the function $F_{\Gamma\Gamma_0}(\mathbf{r}_{N+1})$ is the one-electron wave function describing the scattered electron; and A is an antisymmetrization operator for the electronic coordinates. As the target wave function we used the MRCI wave functions constructed with the direct and indirect DR picture in mind, respectively. The second term, defined as the Q-space portion of the wave function, contains the functions $\Theta_\mu(\mathbf{r}_1,\ldots,\mathbf{r}_{N+1})$, which are square-integrable $N + 1$ configuration state functions that are used to describe short-range correlations and the effects of closed channels. We used the same natural orbitals as those applied in the structure calculations as described in the previous section. The advantage of using natural orbitals is that the orbital space used to generate these states is kept manageable small. The one-electron scattering wave function $F_{\Gamma\Gamma_0}$ is in the case of electron-ion scattering further expanded

as

$$F_{\Gamma\Gamma_0}(\mathbf{r}) = \sum_j c_j^{\Gamma\Gamma_0}\phi_j + \sum_{lm}\left[f_l^{\Gamma}\delta_{ll_0}\delta_{mm_0}\delta_{\Gamma\Gamma_0} + T_{ll_0mm_0}^{\Gamma\Gamma_0}g_l^{\Gamma}\right] \times Y_{lm}(\hat{\mathbf{r}})/r, \quad (3)$$

where $\phi_j(\mathbf{r})$ is a set of square-integrable functions and $f_l^{\Gamma}(k_\Gamma r)$ and $g_l^{\Gamma}(k_\Gamma r)$ are the incoming and outgoing Coulomb functions for a scattered electron with channel momenta k_Γ. In the calculation spherical harmonics Y_{lm} with angular momenta $l \leqslant 6$ and $|m| \leqslant 4$ were included.

By inserting the trial wave function into the complex Kohn functional [9], the unknown coefficients in the trial wave function can be optimized. Also the T matrix elements, $T_{ll_0mm_0}^{\Gamma\Gamma_0}$, for elastic scattering is obtained and by fitting the eigenphase sum of the T matrix to a Breit-Wigner form [12], the energy positions and autoionization widths of the resonant states were determined. These electron scattering calculations are carried out for a fixed geometry of the target ion.

Slightly bigger calculations were made to treat the indirect DR process. In order to be able to perform the scattering calculations, a different expansion basis was used to expand the molecular orbitals. The initial Gaussian basis set was augmented with a small set of diffuse orbitals $(2s,3p,2d)$. As previously discussed [13], due to the relative large dipole moment of H_2O^+, the electron scattering calculations used for modeling the indirect mechanism were carried out with the center of charge of the molecular ion as the origin of the chosen reference frame. Thus, incoming and outgoing Coulomb functions and corresponding spherical harmonics were defined with respect to the center of charge instead of the usual center of mass. Since the effect of rotation of the molecular ion is not included, the cross section for vibrational capture is independent of the choice of the origin.

C. Quasidiabatization

The water molecular ion has the equilibrium bond lengths $R_{OH} = 1.9086a_0$ and a bond angle of $\theta = 108.8^\circ$. As mentioned above, the ionic ground state is dominated by the configuration $(1a_1)^2(2a_1)^2(1b_2)^2(3a_1)^2(1b_1)^1$. In C_s this becomes $(1a')^2(2a')^2(3a')^2(4a')^2(1a'')^1$. When structure calculations are carried out, three types of states are obtained. These are the Rydberg states converging to the ground ionic cores, the states trying to describe the ionization continuum, and the resonant states. Both the Rydberg states and the states describing the ionization continuum have the same configuration as the ground state of the ion plus an outer electron in a diffuse orbital. The resonant states are more or less compact Rydberg states converging to excited ionic cores. These resonant states all have a vacancy in either the $(1b_2)$ or $(3a_1)[(3a')$ or $(4a')$ in $C_s]$ orbitals. By identifying the states with this character, the resonant states can be diabatized relative to the Rydberg states and the ionization continuum. This is done in order to follow the resonant states when they cross the ionic ground state and interact with the Rydberg manifold situated below the ionic potential. This approach is also employed to obtain more data for the potential energy surfaces of the resonant states above the ion and interpolate and extrapolate between the energies of the resonant states calculated using the electron scattering formalism. It should be noted that this approach will provide us with the energy of the resonant state within the energy spread given by the autoionization width. The H_2O system has resonant states that are very narrow and hence the use of structure data to obtain resonant states is relatively accurate.

We have only diabatized the resonant states relative to the Rydberg states by using the CI coefficients. We have not calculated any electronic couplings between the neutral states. In addition, we have not diabatized the resonant states among each other. As will be shown below, there are clear indications of avoided crossings among the resonant states.

III. THEORY

A. Direct process

In our theoretical model of the direct process, the water ion captures an electron and a doubly excited resonant state is formed. Here the dynamics were studied separately for the symmetric and asymmetric motions. In the symmetric mode both OH bond distances vary $R_1 = R_2$, while the H-O-H angle $\theta = 108.8^\circ$ is frozen. When considering the asymmetric motion, $R_1 = 1.9086a_0$ and $\theta = 108.8^\circ$ are frozen, while R_2 varies. Using a time-dependent formalism, this can be described with the initial condition for a wave-packet propagation [14]

$$\Psi_i(R,t=0) = \sqrt{\frac{\Gamma_i(R)}{2\pi}}\chi_{v_i}(R). \quad (4)$$

Here R is a collective notation of the internuclear coordinates, Γ_i is the autoionization width of resonant state i obtained from the electron scattering calculations described above, and χ_{v_i} is the initial vibrational wave function of the water ion.

The dynamics then proceed quasidiabatically along the resonant state

$$i\partial_t\Psi_i(R,t) = \left[\hat{T} + V_i(R) - i\tfrac{1}{2}\Gamma_i(R)\right]\Psi_i(R,t). \quad (5)$$

One-dimensional wave packets were propagated numerically using the Cranck-Nicholson propagation algorithm [15]. Autoionization was here included within the boomerang model [16,17] as a local complex potential.

The wave packets were propagated in time and to prevent reflection toward the end of the grid, a complex absorbing potential was applied at large distances. The contributions to the direct DR cross section from resonant state i were computed with

$$\sigma_i(E) = \frac{2\pi^3}{E}g_i|T_i(E)|^2, \quad (6)$$

where g_i is the ratio of the multiplicity for the final and initial states and E is the electron scattering energy. The transition matrix was obtained [18] using the half Fourier transform of the wave packet at an asymptotic internuclear distance R_c,

$$T_i(E) = \sqrt{\frac{K}{2\pi\mu}}\int_0^\infty \Psi_i(R_c,t)e^{iEt}dt. \quad (7)$$

Here K is the wave number associated with the dissociating fragments and μ is the reduced mass.

No couplings between the neutral states were included in the wave-packet propagation. At low collision energies, some of the resonant states are quasidiabatically not open

for dissociation. This explains some of the sharp thresholds observed in the calculated direct DR cross section (see Sec. IV C). Including electronic couplings between resonant states and also in the Rydberg manifold will allow for a redistribution of flux and open pathways for dissociation at energies below the threshold energy of the resonant state.

B. Indirect process

The approach employed in this work is similar to the one used to calculate the DR cross sections of highly symmetric ions [19,20] as well as of linear polyatomic ions in our recent works [13,21]. Thus, only a brief overview of the theory will be presented.

The starting point is the *ab initio* calculation of the ionic electronic ground state and its series of Rydberg state energies, as described in Sec. II A. As previously suggested in Refs. [22,23], the description of the vibrational dynamics in the simplified model of the indirect process developed by Jungen and Pratt [19,24] considered the electronic capture as the decisive step in the DR mechanism by neglecting autoionization, i.e., assuming that after the neutral molecule is formed all the flux is transferred into the dissociation channels. Hence, the calculated cross section for the indirect DR mechanism provides an upper bound limit because it does not reflect the competition between the dissociation and autoionization channels. Rotation of the molecular target was also neglected, therefore the model only accounts for the electronic and vibrational degrees of freedom. In addition, the cross section was averaged over the energy interval between consecutive resonances leading to a constant probability of electronic capture. Therefore, the cross section will be structureless without the usual rovibrational resonance features. The last simplification was the treatment of the nuclear motion as harmonic, which allows an analytical description of the vibrational states and results in an analytical expression for the final cross section [24].

The cross section can be obtained directly via the low-energy scattering matrix calculated through the variational complex Kohn method. In this approach, the scattering matrix is expressed in the spherical harmonic channel basis as $S^{\alpha}_{ll'mm'} = \langle lm|\hat{S}|l'm'\rangle$, where $Y_{lm}(\theta,\phi) = \langle\theta\phi|lm\rangle$ are centered at a fixed origin in the molecular frame; (θ,ϕ) are polar angles. The indirect DR cross section is given by

$$\langle\sigma\rangle = \frac{\pi}{2E}\sum_{\substack{\alpha\nu_n\\ ll'mm'}} g_\alpha \left|\langle\chi_0|S^{\alpha}_{ll'mm'}|\chi_{\nu_n}\rangle\right|^2\Theta\left(E_{\nu_n}-E\right). \qquad (8)$$

In the above expression, the angular brackets on the left hand side indicate that the cross section is averaged over Rydberg resonances. Since at low energies only the first few vibrational states are important, we can approximate the vibrational wave functions χ_{ν_n} by harmonic oscillators in each of the three normal modes. Therefore, each individual S-matrix element was fitted to a quadratic form simplifying the matrix elements in Eq. (8). We took into consideration only the contribution of transitions from the ground vibrational state to the first and second vibrational states. The cross section is obtained by summing over the electronic symmetry of the scattering wave function α, the different vibrational transitions for the three modes ν_n, and all the elements of the scattering matrix. Here g_α is the multiplicity ratio for the given electronic symmetry. The Heaviside step function guarantees that the contribution to the cross section becomes zero when the electronic energy is greater than the corresponding vibrational threshold E_{ν_n}.

IV. RESULTS

A. Resonant states for direct DR

We show slices of the calculated potential energy surfaces for two cases, the asymmetric and the symmetric modes. When considering the asymmetric motion, $R_1 = 1.9086\ a_0$ and $\theta = 108.8^\circ$ are frozen, while R_2 varies. In the symmetric mode both OH bond distances vary $R_1 = R_2$, while the H-O-H angle $\theta = 108.8^\circ$ is frozen.

By carrying out electron scattering calculations and combining these with the structure calculations, we can extract potential energy surfaces of the resonant states of H_2O. We calculated five resonant states in each of singlet and triplet A' symmetries and two of each singlet and triplet A'' symmetries. These are the resonant states with energies below the first excited state of the ion. As described above, the resonant states were diabatized relative to the Rydberg states converging to the ground ionic core. However, the resonant states were not diabatized relative to each other. In Fig. 1 we display the H_2O resonant states for the asymmetric mode. The energies of the resonant states calculated with the electron scattering calculation are displayed with solid (red) circles. As can be seen, these energies agree very well with energies obtained with structure calculations (shown with red solid curves). Especially at larger distances (roughly $R_2 > 3.0a_0$) one notes that resonances that are Rydberg states converging to excited ionic cores interact with lower resonant states leading to multiple avoided crossings.

In Fig. 2 the states are displayed for the symmetric mode. Here the potential energy surfaces of the lowest two electronic states of the ion are displayed (black thick solid lines) together with the resonant states in C_{2v} (solid colored lines) and C_s (dotted colored lines). We note that in C_{2v} symmetry potentials of resonant states belonging to different irreducible representations cross each other, while the corresponding potentials in C_s symmetry are not allowed to cross. (Note that in this figure, the potential energies of the electronic bound states are not shown.)

As a function of the angle, the potential energy surfaces of the resonant states show clear indications of conical intersections. Similar conical intersections are found among the potential energy surfaces of excited ionic states [25]. Since the resonant states are Rydberg states that converge to the excited ionic cores, the same behavior of the potentials is found for the resonant states. In Fig. 3 the resonant states of $^1A'$ symmetry are plotted as a function of the bending angle, when the bond lengths are frozen at the equilibrium distance. The energies of the resonant states decrease with increasing angle.

The electron scattering calculations provide us with not only the energy positions of the resonant states, but also the autoionization widths. The autoionization widths of the resonant states of H_2O are relatively small. As an example, in

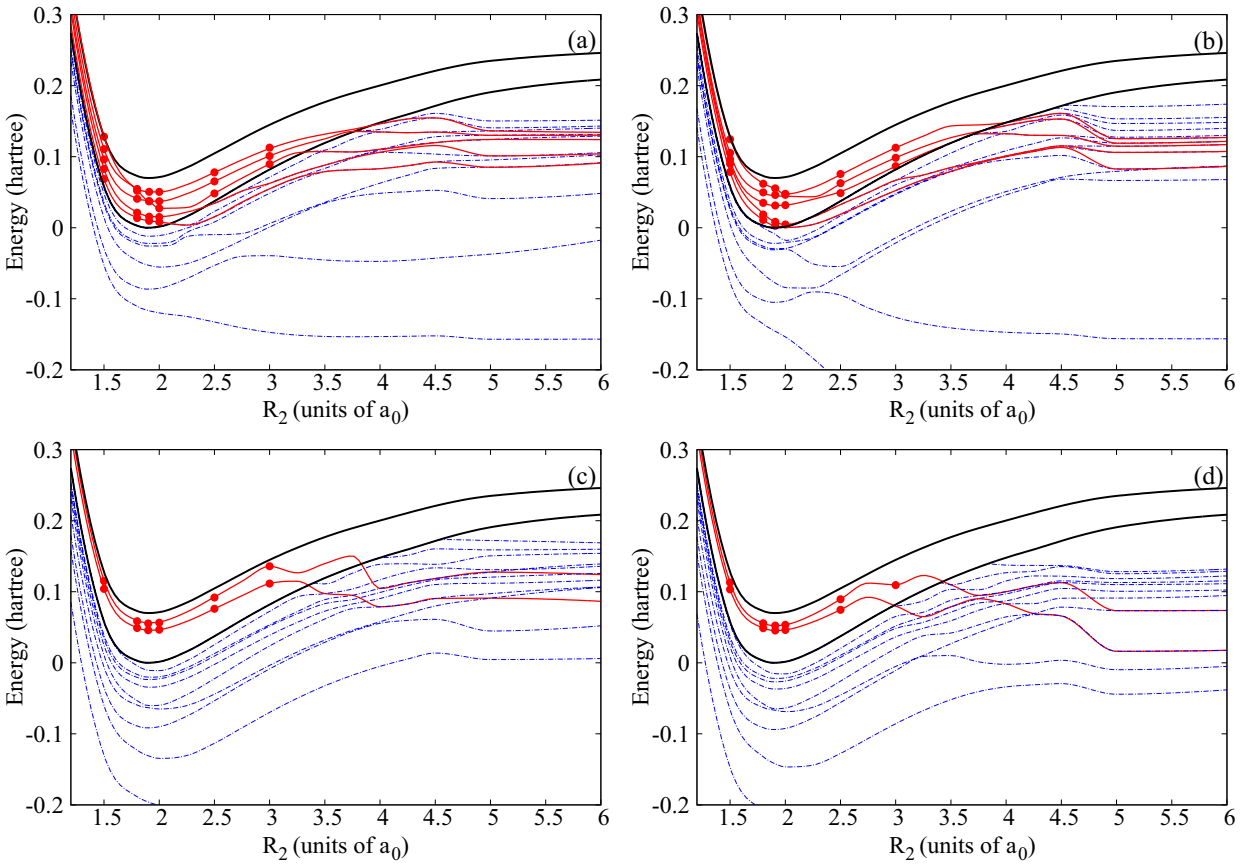

FIG. 1. (Color online) Potentials of H_2O of (a) $^1A'$, (b) $^3A'$, (c) $^1A''$, and (d) $^3A''$ symmetries are displayed as functions of one OH coordinate, while the other OH distance $R_1 = 1.9086a_0$ and the angle $\theta = 108.8^\circ$ are frozen. The potential energy surfaces of the resonant states are shown with solid lines (red online), while the potential of the lowest two electronic states of the ion are displayed with thick solid black lines; the dash-dotted (blue) lines show the potentials of electronic bound states of H_2O.

Fig. 4 the autoionization widths of the resonant states of $^1A'$ symmetry are displayed for the case of asymmetric stretch. It can be noted that the magnitudes of the widths change as the resonant states change character at avoided crossings or conical intersections.

B. Quantum defects and eigenphases: Indirect DR

We have used two main criteria to check the accuracy of our bound-state calculations: the value of the permanent dipole moment and the value of the vibrational frequencies, which are presented in Table I and compared with different values available in the literature. We have also performed a separate coupled-electron-pair approximation (CEPA) calculation using the MOLPRO suite of codes [26] to have another basis for comparison. As can be seen in the table, our MRCI results, which are further used in both Rydberg bound states and continuum scattering calculations, agree well with other studies as well as with our CEPA calculations. Thus, it confirms that a good description of the core ion is achieved, indicating that the interaction potential and exchange with the Rydberg or continuum electron should be correctly represented.

As Sec. II B, we have chosen the center of charge as the origin of the reference frame in the electron scattering calculations. Our choice of origin leads to better convergence of the calculations and a simplification in the analysis of the results as it prevented the asymptotic coupling of partial waves through the long-range anisotropic dipole potential. Once the coupling due to the strong dipole potential is removed, what remain are the nonadiabatic couplings induced by geometry distortions and by the small dipole originating from the changes in geometry. We have extracted the quantum defects from the eigenphases of the scattering matrix given by the complex Kohn method using Seaton's theorem ($S = e^{2i\pi\mu}$) [32]. The eigenphases are extracted at an energy just above the ionization threshold, approximately at 30 meV.

In the left panel of Fig. 5 we show the variation of the quantum defects of the singlet electronic states as functions of the asymmetric stretch normal mode coordinate. The eigenchannel quantum defects vary smoothly with changes in the nuclear mode coordinates. An angular momentum quantum number was assigned to each curve based on the dominant partial wave information extracted from the scattering matrix. Note that as a function of the asymmetric stretch coordinate, the $l = 0$ and 1 quantum defects in $^1A''$ symmetry are not parallel. This is due to the coupling between these states.

The geometry dependence of the quantum defects were obtained using the Rydberg formula

$$V_{n,\alpha}(Q) = V^+(Q) - \frac{1}{2[n - \mu_\alpha(Q)]^2}, \qquad (9)$$

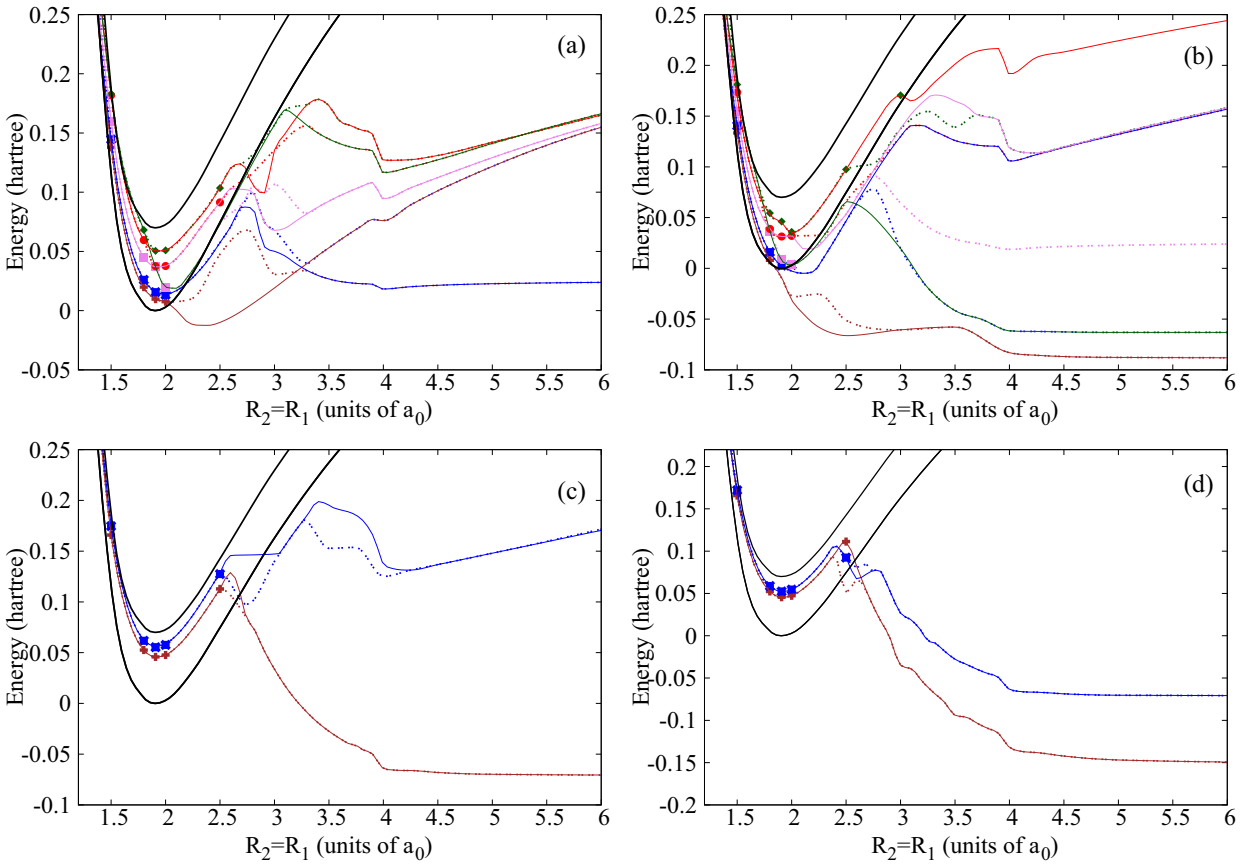

FIG. 2. (Color online) Potential energy surfaces of the H_2O resonant states of (a) $^1A'$, (b) $^3A'$, (c) $^1A''$, and (d) $^3A''$ symmetries are plotted as functions of the OH coordinate where both OH bond distances vary $R_1 = R_2$, while the H-O-H angle $\theta = 108.8^\circ$ is frozen. The solid lines show potential energy surfaces of resonant states in C_{2v} symmetry, while the dotted lines are the potentials of the corresponding states in C_s symmetry. The potentials of the lowest two ionic states are displayed with the black thick solid lines.

where $V^+(Q)$ is the ion energy and $V_{n,\alpha}(Q)$ represents the energy of the Rydberg state $|\alpha\rangle$ with corresponding principal quantum number n. In the right panel of Fig. 5 we show a comparison between these geometry-dependent quantum defects from the bound-state calculations and the eigenphase divided by π from the scattering data. As discussed in Sec. III B, the variation of the quantum defect with the normal mode coordinate determines the indirect DR cross section. The

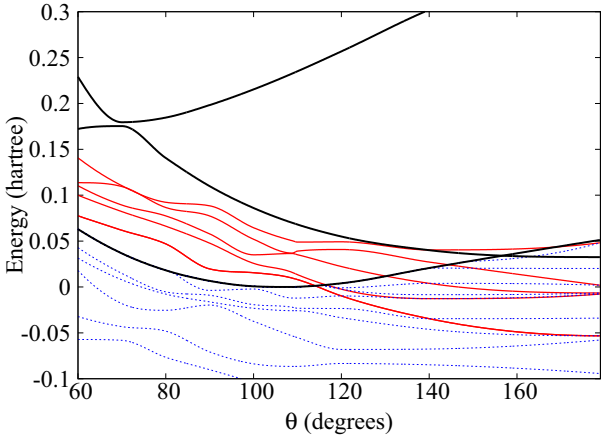

FIG. 3. (Color online) Potential energy surfaces of the resonant states of H_2O of $^1A'$ symmetry as functions of the bending angle and for fixed radial coordinates ($R_{OH} = 1.986a_0$). Also, the potentials of the three lowest ionic states are shown with thick solid lines. Dotted (blue) lines show potential energy surfaces of electronically bound states.

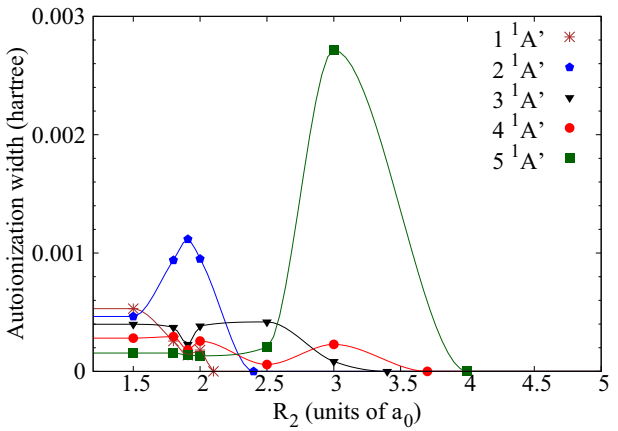

FIG. 4. (Color online) Autoionization widths for the $^1A'$ resonant states of H_2O plotted as functions of one OH coordinate, while the other OH distance $R_1 = 1.9086a_0$ and the angle $\theta = 108.8^\circ$ are frozen.

TABLE I. Vibrational frequencies of the symmetric stretch, bending, and asymmetric stretch normal modes and permanent dipole moments of H_2O^+ obtained in this study. For comparison, other theoretical and experimental results are also shown. Frequencies are given in cm^{-1} and permanent dipole moments μ_e in debye.

Symmetric	Bending	Asymmetric	μ_e	Method	Reference
3339.5	1522.7	3402.7		CEPA	this work
3127.1	1538.9	3454.1	2.37	MRCI	this work
3388	1518	3469		MCSCF CI	Ref. [27]
			2.370	MRD CI	Ref. [28]
3380.6	1476.6	3436.3	2.398	MRCI	Ref. [29]
3182.7	1401.7	3219.5		Expt.	Ref. [30]
3212.9		3259.0		Expt.	Ref. [31]

agreement between the absolute values of the quantum defects is not exact. However, their variations along the normal mode coordinate agree. Therefore, cross sections obtained using quantum defects from bound Rydberg state calculations or obtained from the electron scattering calculations should be nearly identical. The indirect DR cross section was calculated using Eq. (8) [13] with the S matrix obtained from the electron scattering calculations.

Extensive theoretical studies of the water Rydberg states have been carried out by Child and co-workers [33–36]. The quantum-defect functions were then generated by fitting a quantum-defect matrix to *ab initio* potential energy surfaces obtained using the configuration-interaction method. As an example, the eigenquantum defects for Rydberg states of $^1B_1$ symmetry at approximately the equilibrium geometry of the water ion obtained by Theodorakopoulos *et al.* [34] are 1.44, 0.05, and 0.75. These should be compared with the numbers 1.49, 0.10, and 0.67 obtained here with the electron scattering calculation.

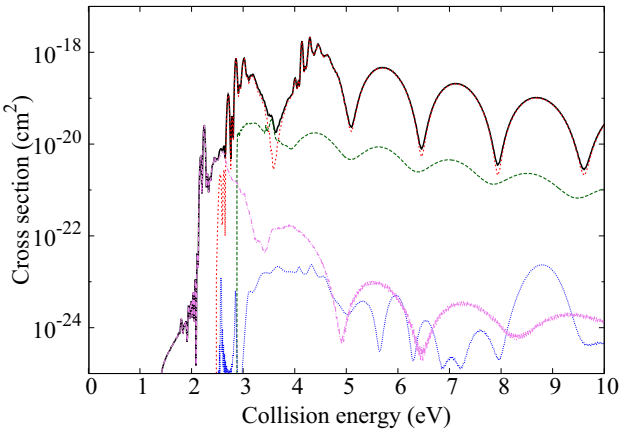

FIG. 6. (Color online) Direct DR cross section for the asymmetric stretch dissociation. Colored lines show total direct contributions from resonant states of different electronic symmetries.

C. Cross sections: Direct and indirect DR

The cross section for direct DR is calculated for both the asymmetric and symmetric stretches where either one or both OH bonds break. For the asymmetric stretch, the electronic resonant states of H_2O are not open for dissociation at low collision energies. An energy larger than 2 eV is needed to break the bond if the states are followed quasidiabatically as described above. Figure 6 shows the cross section for direct DR when only one the OH bonds breaks. The resonant states produce cross sections with sharp peaks and oscillations. Some of the peaks can be explained by tunneling resonances (shape resonances) formed by barriers in the potential energy curves. As seen for other systems, the regular oscillations above 4 eV are due to energy dependence of the electron capture probability [37,38]. For collision energies below 3 eV electronic resonant states of $^3A''$ symmetry dominate, while above this energy, $^3A'$ states become important.

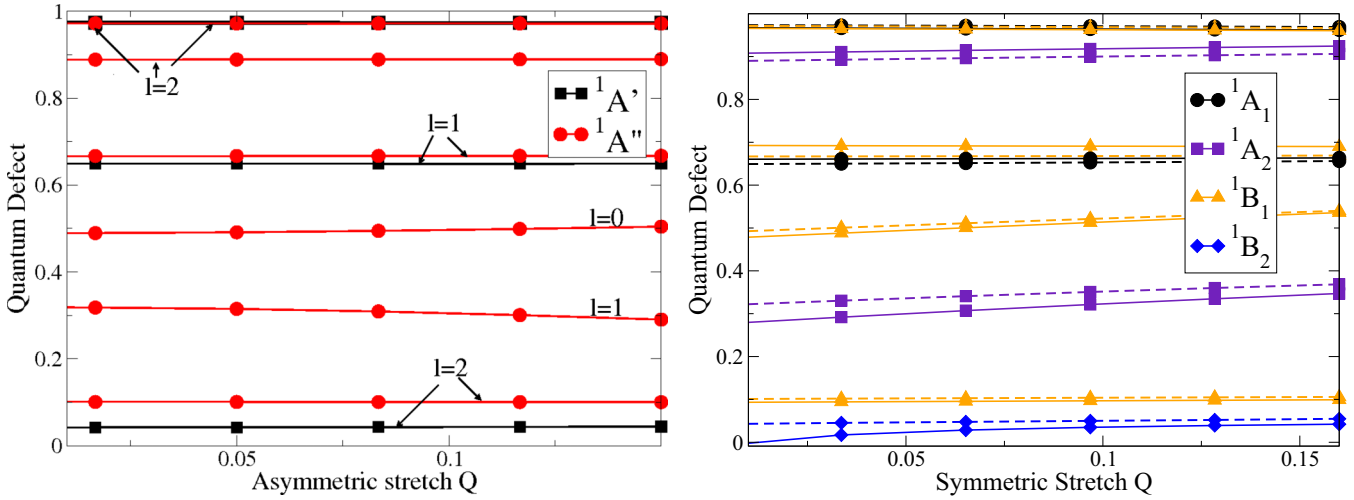

FIG. 5. (Color online) Shown on the left are quantum defects for singlet electronic states as a function of the asymmetric stretch vibrational mode. The plot shows the variation of the quantum defect with respect to the normal mode coordinate Q (in a.u. amu$^{1/2}$) and the different angular momentum values associated with each state. On the right is an example of the agreement between the geometry-dependent quantum defects obtained from our bound-state calculations (solid lines) and the eigenphase shifts, divided by π, from our scattering results (dashed lines) as a function of the symmetric stretch normal mode coordinate.

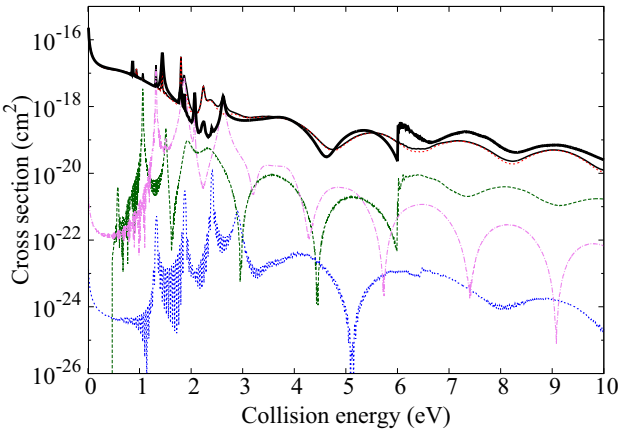

FIG. 7. (Color online) Direct DR cross section for the symmetric stretch where the resonant states have been followed in C_s (black solid line) or C_{2v} (black dashed line) symmetries. Colored lines show the total direct contribution from C_s resonant states of the different electronic symmetries.

The calculation of the direct DR cross section for the symmetric stretch can be computed by following resonant states in either C_s or C_{2v} symmetry. In Fig. 7 we compare the total cross section calculated with the two symmetries. For resonant states of C_s symmetry, we display the contributions from the different irreducible representations. When both bonds break some resonant states are open for dissociation at low collision energies. Most important are resonant states of $^3A'$ symmetry and it is the lowest resonant state of this symmetry driving the direct electron capture at low energies. When the states are diabatized conserving the C_{2v} symmetry, the direct DR cross section does not significantly change compared to the C_s result. There are some differences in the cross sections at larger energies where the higher-lying resonant states contribute.

The indirect DR cross section has been calculated up to the energy that corresponds to $v = 2$ of the asymmetric stretch threshold, as shown in Fig. 8. The sharp drop in the energy dependence of the indirect cross section results from the thresholds of the $v = 1$ and 2 levels of the three normal modes of H_2O^+, as given by the expression (8). For comparison, we have also plotted the data reported from a single-pass merged beam measurement [1] and the results obtained in the ASTRID [2] and CRYRING [3] storage ring experiments. The cross section taken from the merged-beam measurement needed to be divided by 2 due to an error in their calibration procedure, as reported latter by Mitchell [39]. The ion-storage ring data shown in the figure are the measured rate coefficient divided by the velocity $\langle\sigma\rangle = \langle v\sigma\rangle/v$. This will deviate from the cross section when the collision energy is comparable to the energy spread of the electrons [2]. At low collision energies where the indirect process dominates, computed and measured cross sections are in fairly good agreement. Above 1 meV, the calculated indirect cross section is larger than the experimental results. This is an expected behavior since in our theoretical model we neglect autoionization under the assumption that predissociation takes place on a much faster time scale.

At low energies the cross sections from the two ion-storage ring experiments have been fitted to stronger energy

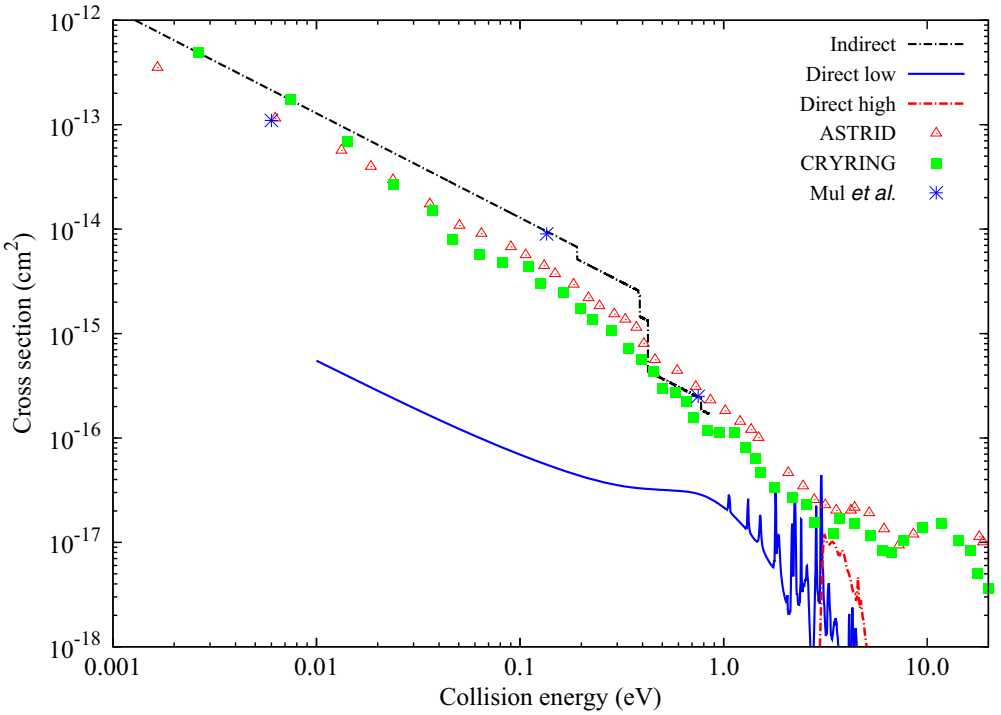

FIG. 8. (Color online) Calculated cross sections for indirect and direct DR are compared with the results from the ion-storage rings ASTRID [2] and CRYRING [3], as well as the single-pass merged electron-ion beams [1] (this cross section has been divided by 2). The contributions from the resonant states lying below the first excited state of the ion (direct low) are shown separately from the contributions from higher-lying resonant states (direct high).

dependences than the E^{-1} dependence, as predicted by Wigner's threshold law [40]. The CRYRING team reported a $E^{-1.24}$ behavior [3], while ASTRID found a cross section that goes like $E^{-1.35}$ [2]. This steeper slope has been attributed to the presence of an indirect mechanism driving the DR reaction [3]. We indeed find the indirect mechanism to be important at low energies. However, by definition, our cross section calculated with the simplified model has the form $(a_1 + a_2 + a_3)E^{-1}$, where the a_i coefficients are related to the factors (capture probabilities) relevant to each normal mode q_i. Therefore, even though our cross section is the result of a pure indirect DR mechanism, it cannot reproduce the steep slopes found in the storage ring measurements. The theory predicts drops in the cross section at energies corresponding to the vibrational threshold energies. The storage ring experiments show no drop near the $v = 1$ threshold for the bend, but do for the $v = 1$ symmetric and asymmetric stretches and $v = 2$.

In Fig. 8 the total cross section for the direct DR along the symmetric and asymmetric stretches is included. Both calculations are performed following the resonant states in C_s symmetry. The direct electron capture and dissociation along resonant states contribute to the low-energy DR cross section when both bonds simultaneously break. At low energies, the cross section from the direct mechanism is, however, almost two orders of magnitude smaller than the indirect one. The direct DR cross section calculated for the asymmetric stretch, where only one of the OH bonds breaks, contributes to the DR cross section for energies above 1 eV where the resonant states are open for dissociation. The calculated one-dimensional direct DR cross section is significantly smaller than the measured cross sections. In this case, we treated the direct and indirect mechanisms as independent processes. These should be treated together and couplings between the states involved should be considered. This will produce new pathways to dissociation resulting in a larger cross section and less-pronounced structures. In addition, including several dimensions will also softening these sharp peaks.

At higher scattering energies, the direct cross section due to the resonant states with energies below the first excited state of the ion drops. The direct cross section in this region ($E > 1.9$ eV) arises from capture into higher resonant states that lie above the first excited state of the ion. In order to estimate the contributions from these higher resonant states, it is necessary to include two target channels in the electron scattering calculations and also to compute not only the total autoionization width, but the partial width [41]. We carried out additional calculations to determine the energies and widths of several of these resonant states with vertical excitation energies less than 5 eV. We use this molecular data as input for wave-packet calculations. The contributions to the DR cross section from these states peak in the vicinity of the measured high-energy structure at 5 eV, as can be seen in Fig. 8. The experiments also observe a peak around 15 eV. This is due to higher-lying resonant states not considered in the present study.

V. CONCLUSION

Potential energy surfaces, autoionization widths, and elements of the scattering matrix were obtained by combining structure with electronic scattering calculations at the MRCI level of theory. Calculations on the direct and indirect mechanisms of dissociative recombination of H_2O^+ were performed. One-dimensional wave-packet studies of direct dissociation along electronic resonant states were performed to estimate the cross section for direct DR. The contribution to the low-energy cross section from the direct mechanism was found when both bonds simultaneously break. At collision energies above 1 eV, also the two-body fragmentation seems to be important.

The indirect mechanism was modeled by performing a vibrational frame transformation of the scattering matrix elements obtained at low collision energies (where resonant states do not contribute). The model neglects the contribution from autoionization and only includes contributions from the $v = 1$ and 2 vibrational states. The calculation shows that the indirect mechanism is clearly important at electron collision energies less than 1 eV. At low collision energies the indirect DR cross section is slightly larger than measured ones and it drops at the opening of vibrationally excited states of the target ion.

Strong couplings are observed between the Rydberg states that mediate the indirect process and the dissociative resonant states. In order to obtain branching ratios and fragmentation patterns, multidimensional dynamics including the couplings must be done.

ACKNOWLEDGMENTS

This work was supported by the National Science Foundation, Grant No. PHY-11-60611. In addition some of this material was based on work done while A.E.O. was serving at the NSF. Å.L. acknowledges support from the Swedish Research council, Grant No. 2014-4164 and the Carl-Trygger Foundation.

[1] P. M. Mul, J. W. McGowan, P. Defrance, and J. B. A. Mitchell, J. Phys. B **16**, 3099 (1983).

[2] M. J. Jensen, R. C. Bilodeau, O. Heber, H. B. Pedersen, C. P. Safvan, X. Urbain, D. Zajfman, and L. H. Andersen, Phys. Rev. A **60**, 2970 (1999).

[3] S. Rosén, A. Derkatch, J. Semaniak, A. Neau, A. Al-Khalili, A. Le Padellec, L. Vikor, R. Thomas, H. Danared, M. af Ugglas, and M. Larsson, Faraday Disc. **115**, 295 (2000).

[4] S. Datz, G. Sundström, C. Biedermann, L. Broström, H. Danared, S. Mannervik, J. R. Mowat, and M. Larsson, Phys. Rev. Lett. **74**, 896 (1995).

[5] L. Vikor, A. Al-Khalili, H. Danared, N. Djurić, G. H. Dunn, M. Larsson, A. Le Padellec, S. Rosén, and M. af Ugglas, Astron. Astrophys. **344**, 531 (1999).

[6] Å. Larson, A. Le Padellec, J. Semaniak, C. Strömholm, M. Larsson, S. Rosén, R. Peverall, H. Danared, N. Djurić, G. H. Dunn, and S. Datz, Astrophys. J. **505**, 459 (1998).

[7] S. Datz, R. Thomas, S. Rosén, M. Larsson, A. M. Derkatch, F. Hellberg, and W. van der Zande, Phys. Rev. Lett. **85**, 5555 (2000).
[8] R. Thomas, S. Rosén, F. Hellberg, A. Derkatch, M. Larsson, S. Datz, R. Dixon, and W. J. van der Zande, Phys. Rev. A **66**, 032715 (2002).
[9] T. N. Rescigno, C. W. McCurdy, A. E. Orel, and B. H. Lengsfield III, in *Computational Methods for Electron-Molecule Scattering*, edited by W. M. Huo and F. A. Gianturco (Plenum, New York, 1995).
[10] T. H. Dunning, Jr., J. Chem. Phys. **90**, 1007 (1989).
[11] K. Kaufmann, W. Baumeister, and M. Jungen, J. Phys. B **22**, 2223 (1989).
[12] S. Geltman, *Topics in Atomic Collision Theory* (Academic, New York, 1997), p. 31.
[13] S. Fonseca dos Santos, N. Douguet, V. Kokoouline, and A. E. Orel, J. Chem. Phys. **140**, 164308 (2014).
[14] C. W. McCurdy and J. L. Turner, J. Chem. Phys. **78**, 6773 (1983).
[15] A. Goldberg, H. M. Schey, and J. L. Schwartz, Am. J. Phys. **35**, 177 (1967).
[16] A. Herzenberg, J. Phys. B **1**, 548 (1968).
[17] L. Dubé and A. Herzenberg, Phys. Rev. A **20**, 194 (1979).
[18] P. L. Gertitschke and W. Domcke, Phys. Rev. A **47**, 1031 (1993).
[19] C. Jungen and S. T. Pratt, Phys. Rev. Lett. **102**, 023201 (2009).
[20] N. Douguet, V. Kokoouline, and A. E. Orel, J. Phys. B **45**, 051001 (2012).
[21] N. Douguet, S. Fonseca dos Santos, V. Kokoouline, and A. E. Orel, EPJ Web Conf. **84**, 07003 (2015).
[22] I. A. Mikhaylov, V. Kokoouline, Å. Larson, S. Tonzani, and C. H. Greene, Phys. Rev. A **74**, 032707 (2006).
[23] V. Kokoouline, N. Douguet, and C. H. Greene, Chem. Phys. Lett. **507**, 1 (2011).
[24] C. Jungen and S. T. Pratt, J. Chem. Phys. **129**, 164311 (2008).
[25] J. Suárez, L. Méndez, and I. Rabadán, J. Phys. Chem. Lett. **6**, 72 (2015).
[26] H.-J. Werner, P. J. Knowles, R. Lindh, F. R. Manby, M. Schütz *et al.*, MOLPRO, version 2008.3, a package of *ab initio* programs (2008).
[27] P. J. Fortune, B. J. Rosenberg, and A. C. Wahl, J. Chem. Phys. **65**, 2201 (1976).
[28] S. Wu *et al.*, J. Mol. Spectrosc. **225**, 96 (2004).
[29] B. Weiss, S. Carter, P. Rosmus, H.-J. Werner, and P. J. Knowles, J. Chem. Phys. **91**, 2818 (1989).
[30] D. Forney, M. E. Jacox, and W. E. Thompson, J. Chem. Phys. **98**, 841 (1992).
[31] T. R. Huet, C. J. Pursell, W. C. Ho, B. M. Dinelli, and T. Oka, J. Chem. Phys. **97**, 5977 (1992).
[32] M. J. Seaton, Rep. Prog. Phys. **46**, 167 (1983).
[33] I. D. Petsalakis, G. Theodorakopoulos, and M. S. Child, J. Phys. B **28**, 5179 (1995).
[34] G. Theodorakopoulos, I. D. Petsalakis, and M. S. Child, J. Phys. B **29**, 4543 (1996).
[35] M. S. Child, Philos. Trans. R. Soc. London Ser. A **355**, 1623 (1997).
[36] M. S. Child, J. Chem. Phys. **112**, 3754 (2000).
[37] O. Motapon, M. Fifirig, A. Florescu, F. O. Waffeu Tamo, O. Crumeyrolle, G. Varin-Bréant, A. Bultel, P. Vervisch, J. Tennyson, and I. F. Schneider, Plasma Sources Sci. Technol. **15**, 23 (2006).
[38] J. B. Roos, Å. Larson, and A. E. Orel, Phys. Rev. A **78**, 022508 (2008).
[39] J. B. A. Mitchell, Phys. Rep. **186**, 215 (1990).
[40] E. P. Wigner, Phys. Rev. **73**, 1002 (1948).
[41] A. E. Orel, K. C. Kulander, and T. N. Rescigno, Phys. Rev. Lett. **74**, 4807 (1995).